

# Mucin-Inspired, High Molecular Weight Virus Binding Inhibitors Show Biphasic Binding Behavior to Influenza A Viruses


Matthias Wallert, Chuanxiong Nie, Parambath Anilkumar, Srinivas Abbina, Sumati Bhatia, Kai Ludwig, Jayachandran N. Kizhakkedathu, Rainer Haag,\* and Stephan Block\*

Multivalent binding inhibitors are a promising new class of antivirals that prevent virus infections by inhibiting virus binding to cell membranes. The design of these inhibitors is challenging as many properties, for example, inhibitor size and functionalization with virus attachment factors, strongly influence the inhibition efficiency. Here, virus binding inhibitors are synthesized, the size and functionalization of which are inspired by mucins, which are naturally occurring glycosylated proteins with high molecular weight (MDa range) and interact efficiently with various viruses. Hyperbranched polyglycerols (hPGs) with molecular weights ranging between 10 and 2600 kDa are synthesized, thereby hitting the size of mucins and allowing for determining the impact of inhibitor size on the inhibition efficiency. The hPGs are functionalized with sialic acids and sulfates, as suggested from the structure of mucins, and their inhibition efficiency is determined by probing the inhibition of influenza A virus (IAV) binding to membranes using various methods. The largest, mucin-sized inhibitor shows potent inhibition at pM concentrations, while the inhibition efficiency decreases with decreasing the molecular weight. Interestingly, the concentration-dependent IAV inhibition shows a biphasic behavior, which is attributed to differences in the binding affinity of the inhibitors to the two IAV envelope proteins, neuraminidase, and hemagglutinin.

## 1. Introduction

Viral infections and resulting pandemics are a human danger and repeatedly get into the focus due to the circulation of newly emerging viruses, such as Zika, influenza, and corona viruses<sup>[1–3]</sup> The development of antivirals to fight viral infections is often a time-consuming process and the generated drugs are often effective only for a certain period of time as mutation of the targeted virus may cause the developed antiviral to become ineffective, for example due to occurrence of resistance.<sup>[4]</sup> Hence, antivirals targeting highly conserved structures of viruses, such as the envelope proteins that are involved in virus binding to the membrane of the host cell, are entering more and more the focus of current research.<sup>[5,6]</sup> As virus binding proteins typically show a very weak affinity to their native attachment factors on the cell membrane,<sup>[7]</sup> viruses bind to cells by forming many protein-receptor interactions in parallel,

M. Wallert, Dr. S. Block  
Institute of Chemistry and Biochemistry  
Emmy-Noether Group “Bionanointerfaces”  
Freie Universität Berlin  
Takustr. 3, Berlin 14195, Germany  
E-mail: stephan.block@fu-berlin.de  
C. Nie, Dr. S. Bhatia, Prof. R. Haag  
Institute of Chemistry and Biochemistry  
Macromolecular Chemistry  
Freie Universität Berlin  
Takustr. 3, Berlin 14195, Germany  
E-mail: haag@zedat.fu-berlin.de

 The ORCID identification number(s) for the author(s) of this article can be found under <https://doi.org/10.1002/smll.202004635>.

© 2020 The Authors. Published by Wiley-VCH GmbH. This is an open access article under the terms of the Creative Commons Attribution License, which permits use, distribution and reproduction in any medium, provided the original work is properly cited.

Dr. P. Anilkumar, Dr. S. Abbina, Prof. J. N. Kizhakkedathu  
Centre for Blood Research  
Life Sciences Institute  
Department of Pathology and Laboratory Medicine  
University of British Columbia  
2350 Health Sciences Mall, Vancouver, British Columbia V6T 1Z3, Canada  
Dr. K. Ludwig  
Research Center for Electron Microscopy and Core Facility BioSupraMol  
Institute of Chemistry and Biochemistry  
Freie Universität Berlin  
Fabeckstr. 36a, Berlin 14195, Germany  
Prof. J. N. Kizhakkedathu  
Department of Chemistry  
University of British Columbia  
Vancouver, British Columbia V6T 1Z3, Canada  
Prof. J. N. Kizhakkedathu  
School of Biomedical Engineering  
University of British Columbia  
Vancouver, British Columbia V6T 1Z3, Canada

DOI: 10.1002/smll.202004635

thereby generating a multivalent interaction to the cell membrane.<sup>[8]</sup> This first step in the infection cycle of cells can be inhibited by addition of multivalent binding inhibitors.<sup>[5,9]</sup>

The design of multivalent virus binding inhibitors is complicated by the fact that many properties, such as inhibitor size and functionalization with virus attachment factors, have a strong impact on the inhibition efficiency,<sup>[10]</sup> making the process of finding inhibitor designs with high inhibition efficiency a time-consuming matter. Nevertheless, the concept of using multivalent interactions to hinder binding of infectious agents (viruses and bacteria) to cells is already implemented in nature by the biological hydrogel mucus, which covers almost all epithelia cells.<sup>[11]</sup> It forms the first defense barrier against viruses and bacteria by capturing such infectious agents before they are able to reach to the cell surface.<sup>[12]</sup> Mucus is formed by dynamic cross-linking of mucins, which are highly glycosylated proteins having molecular weights ranging between 0.1 and few MDa and bind with high specificity and selectivity to viruses while allowing other species (e.g., nutrients) to pass the hydrogel.<sup>[11,13]</sup> As mucins are effective binders of various virus species, our study aims to synthesize virus binding inhibitors, the size and functionalization of which is inspired by mucins, thereby allowing for potent and potentially broad band inhibition of virus binding.

In particular, we aim to generate multivalent virus binding inhibitors reaching molecular weights on the MDa scale, which is a value being in the middle of the weight range reported for mucins.<sup>[13]</sup> Besides mimicking the size of mucins, such large values are further motivated by the observation that the size of a binding inhibitor has a strong impact on its efficiency to bind to viruses,<sup>[10]</sup> which led to the suggestion that the optimal size of a virus binding inhibitor is approximately one third of the size of the virus to be inhibited. As many viruses are within the size range of 30–200 nm, the size of the virus inhibitor should therefore be on the order of a few tens of nanometers, corresponding to polymer scaffolds with a molecular weight hitting the MDa scale. Besides size, the functionalization of the inhibitor is also known to be an important determinant for the strength of the virus-inhibitor interaction. Mucins present a high amount of terminal sialic acid and sulfate moieties,<sup>[12]</sup> which are known to play a role in the binding of various viruses. This motivates to functionalize the virus binding inhibitor with sialic acid and sulfate groups (at degrees of functionalization comparable to mucins) to ensure efficient binding to viruses, thereby offering the perspective to provide broad band virus binding inhibition activity.

The performance of the synthesized, mucin-inspired virus binding (MuVib) inhibitors is investigated by probing the binding inhibition of a H3N2 influenza A virus (IAV) strain using various assays, including a new binding assay based on total internal fluorescence (TIRF) microscopy. MuVib inhibitors with molecular weights ranging between 10 and 2600 kDa are synthesized, which allows to probe the inhibition efficiency as a function of inhibitor size.

## 2. Results and Discussion

The aim of this study is to synthesize virus binding inhibitors, the size and functionalization of which have been motivated

by mucins. With respect to size, this aim requires to synthesize macromolecules having molecular weights on the MDa scale, which can then serve as scaffold for further functionalization with virus attachment factors. Recent studies have demonstrated the synthesis of virus inhibitors hitting the MDa range, which were based on polyacrylamide, polyamidoamine, polyethylene imine or copolymers of them,<sup>[14]</sup> but showed only little biocompatibility due to their positive charges. In order to generate a high molecular weight (MDa-sized) multivalent virus binding inhibitor, we therefore decided to use hyperbranched polyglycerols (hPG), which are known to be highly biocompatible and the synthesis of single hPG molecules with molecular weights of several 100 kDa has recently been demonstrated.<sup>[15,16]</sup> The strategy for the synthesis of MDa-sized hPG molecules for use as mucin-inspired virus binding (MuVib) inhibitor is shown in **Figure 1a**. In addition to this inhibitor, hPGs with lower molecular weights (ranging between 10 and 500 kDa) have been synthesized, which allows for investigating the effect of the inhibitor size on the inhibitor efficiency as suggested in a recent work by Vonnemann et al.<sup>[10]</sup> While single hPG molecules up to 600 kDa can be synthesized in a single step,<sup>[17]</sup> the synthesis of the 2600 kDa hPG molecules required an additional step, in which 600 kDa hPGs served as macroinitiator for a further polymerization (**Figure 1a**) to generate a mucin-sized polymer.<sup>[16]</sup> This approach yielded 4 different hPG scaffolds with molecular weights of 10, 100, 500, and 2600 kDa (**Table 1**). DLS measurements yielded hydrodynamic diameter of ≈6 nm (10 kDa), 9 nm (100 kDa), 13 nm (500 kDa), and 29 nm (2600 kDa), respectively.

Besides size, the functionalization of a polymer scaffold surface with chemical groups is also an important parameter for its efficiency to serve as virus inhibitor, as it determines the amount and strength of interactions formed between a virus and the inhibitor.<sup>[7]</sup> In this work, the hPG-based inhibitors were functionalized with sialic acids (SAs) and sulfate groups, which is motivated by the fact that many terminal glycans in mucins terminate either with a sialic acid (SA) or a sulfate group.<sup>[13]</sup> Furthermore, both groups are known attachment factors for various viruses:<sup>[18]</sup> SAs are, for example, involved in the attachment of influenza virus and many corona virus strains,<sup>[19,20]</sup> while viruses such as the vesicular stomatitis virus or herpes simplex virus bind to sulfated glycosaminoglycans.<sup>[21,22]</sup> As these two chemical groups already enable interaction with various virus species, we simplified the complex structure of mucins by regarding only these two terminal functional groups and thus by functionalizing the hPG scaffolds with SAs and sulfate residues as shown in **Figure 1b**.

Various values for the content of SA and sulfate groups in mucins have been reported in the literature, typically ranging between 4–20 wt% for sialic acid and 1.2–11.9 wt% for sulfates.<sup>[23,24]</sup> In this study, 5 mol% of the hydroxyl groups were substituted with SA and sulfate moieties (**Figure 1b**), respectively, which resulted in 15 wt% SA and 5 wt% sulfate (**Table 1**), being close to the middle of the ranges reported for mucins. In addition, for the 2600 kDa inhibitor two control polymers were prepared, carrying only one of the two moieties. All functionalized inhibitors show a negative zeta potential ranging from –22 to –27 mV (**Table 1**), which is caused by the incorporation the negatively charged sulfate and SA moieties. Both,

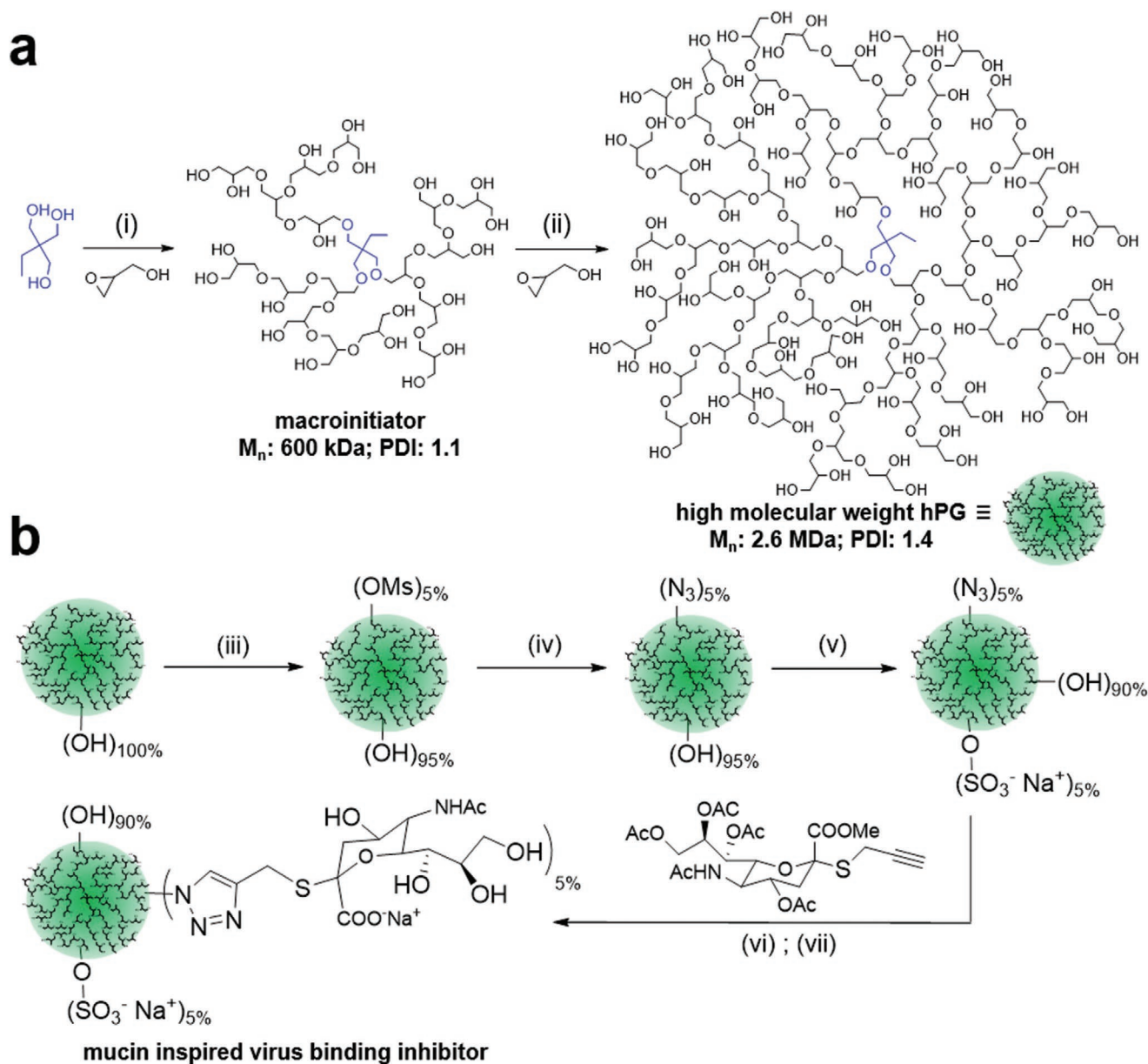


**Figure 1.** Synthesis of mucin-inspired virus binding (MuVib) inhibitors based on high-molecular weight hPG. a) Polymerization of the MDa hPG in two steps i) potassium methoxide in dry 1,4 dioxane at 95 °C and glycidol addition (0.5 mL h<sup>-1</sup>), ii) potassium hydride in dry DMF at 95 °C and glycidol addition (0.9 mL h<sup>-1</sup>). b) Functionalization of the MDa hPG, all reactions were carried out in dry DMF under argon atmosphere, iii) mesylation with mesyl chloride and triethylamine at room temperature for 20 h, iv) azidation using sodium azide at 80 °C for 20 h, v) sulfation with sulfur trioxide pyridine complex at 60 °C for 20 h, vi) copper-catalyzed alkyne-azide cycloaddition using copper sulfate pentahydrate, sodium ascorbate at 50 °C for 20 h, vii) deprotection with sodium hydroxide at room temperature for 2 h.

unfunctionalized and functionalized hPG polymers are highly water soluble. Furthermore, a predominantly spherical morphology of the MuVib inhibitor was verified using cryo-electron microscopy (see Figure S1, Supporting Information).

In a next step, we assessed the applicability of the synthesized inhibitors to hinder binding of viruses to cell membranes. These investigations were done using influenza A virus (IAV), being a highly important representative of the viruses that bind to cells via SAs. In particular, we employed the IAV strain X31 (H3N2), which is often used for assessing the efficiency of IAV

binding inhibition and thus allows for comparing the measured inhibition efficiency with literature values.<sup>[25–27]</sup> Interestingly, two membrane proteins are involved in this binding process of all IAVs: Hemagglutinin (HA) and neuraminidase (NA). Both proteins are able to interact with SAs, but while HA is known to promote IAV attachment to the cell membrane, NA is known to possess SA cleavage activity and is therefore believed to promote IAV egress (after the virus replication cycle has been completed).<sup>[28–30]</sup> The interplay between HA and NA is known to be important for completion of the virus life cycle and started

**Table 1.** Properties of synthesized virus binding inhibitors based on hPG.

	$d^a)$	$\zeta\text{-pot.}^b)$	$\text{SO}_4^c)$		$\text{SA}^c)$		$n_{\text{sulfate}}^d)$	$n_{\text{SA}}^d)$
	[nm]	[mV]	[mol%]	[wt%]	[mol%]	[wt%]	[-]	[-]
hPG <sub>10</sub> -SA-SO <sub>4</sub>	4.9 ± 4.2	-26.3 ± 0.9	7.2	6.2	7.0	19.3	7	7
hPG <sub>100</sub> -SA-SO <sub>4</sub>	12.0 ± 7.2	-22.4 ± 1.0	5.0	4.7	5.5	16.5	68	75
hPG <sub>500</sub> -SA-SO <sub>4</sub>	16.3 ± 9.7	-24.3 ± 0.8	3.9	3.7	5.7	17.1	268	392
hPG <sub>2600</sub> -SA-SO <sub>4</sub>	28.1 ± 17.1	-26.8 ± 1.1	5.0	4.7	5.6	16.7	1724	1931
hPG <sub>2600</sub> -SA	29.2 ± 15.3	-23.4 ± 0.5	-	-	5.6	17.7	-	1931
hPG <sub>2600</sub> -SO <sub>4</sub>	20.8 ± 11.4	-17.1 ± 0.9	4.3	5.3	-	-	1482	-
hPG <sub>2600</sub>	28.9 ± 14.9	9.5 ± 0.5	-	-	-	-	-	-

<sup>a)</sup>Hydrodynamic diameter obtained by DLS at sample concentration of 1 mg mL<sup>-1</sup> in PBS (10 mM, pH 7.4); <sup>b)</sup>Zeta-potential measurement in 10 mM phosphate buffer (pH 7.4); <sup>c)</sup>amount of converted hydroxyl groups in percent, determined by elemental analysis, degree of sialic acid based on fully conversion of azide moieties; <sup>d)</sup>calculated number of sialic acid and sulfate per polymer based on  $M_n$ .

to attract the focus of recent research.<sup>[31]</sup> According to Harris et al.<sup>[32]</sup> there are ≈300 copies of HA compared to 50 copies of NA in the membrane of the influenza A virus strain X31. To prevent NA-mediated cleavage of SAs at our synthesized binding inhibitor, a thioether bond was used to link the sialic acid to the polymer scaffold, which cannot be cleaved by NA.

In this study, the inhibitor performance was first investigated using the hemagglutination inhibition (HAI) assay (Figure S2, Supporting Information), which takes advantage of the feature that red blood cells become crosslinked upon interaction with IAVs (called hemagglutination).<sup>[33]</sup> By addition of virus binding inhibitors, the interaction between the virus and the membranes of red blood cells can be inhibited and the lowest inhibitor concentration at which no agglutination occurs anymore is defined as (HAI assay-derived) inhibition constant  $k_i$ . This assay is a well-established means for determining the amount of inhibitor (concentration) that has to be added in order to efficiently inhibit IAV binding to RBC membranes.<sup>[34]</sup> For the 10 and 100 kDa inhibitors we observed  $k_i$  values in the low μM range (Table 2), whereas the 500 kDa inhibitor approached the nM range and the most potent inhibition was exhibited by the 2600 kDa MuVib inhibitor (31 pM; 0.1 μg mL<sup>-1</sup>), irrespective if this hPG was functionalized with SA and SO<sub>4</sub> or SA alone. The inhibitors lacking SA (i.e., the sulfated hPGs) showed no notable inhibition.

Although the HAI assay is often used to assess the inhibitory potential of compounds, it does not allow to directly probe the interaction of IAVs with their attachment factors or how

this interaction is altered by addition of inhibitors. In order to obtain such information, we extended a recently introduced virus-membrane binding assay based on total internal reflection fluorescence (TIRF) microscopy (Figure 2).<sup>[35]</sup> In this assay, a supported lipid bilayer (SLB), which is supplemented with the attachment factor of the virus of interest, is formed at a glass interface and the (transient) binding of fluorescently labeled viruses to the SLB is monitored using TIRF microscopy (Figure 2a). By choosing TIRF illumination, the excitation light hits the SLB-glass interface at the critical angle of total internal reflection, which generates an evanescent wave with a penetration depth of ≈100–150 nm,<sup>[36]</sup> so that fluorescence is only excited in very close vicinity of the SLB. Hence, to resolve fluorescently labeled viruses for an appreciable time period in TIRF microscopy, they have to be bound to the SLB, while unbound viruses are not visible.

For probing the IAV-SA interaction, a SLB based of POPC (96.2 wt%, 1-palmitoyl-2-oleoyl-glycero-3-phosphocholine) and DSPE-PEG2k (3.8 wt%, 1 mol%, 1,2-distearoyl-sn-glycero-3-phosphoethanolamine-*N*-[carboxy(polyethylene glycol)-2000] (sodium salt)) was supplemented with the ganglioside GD1a (2.5 wt%, 1 mol%), which presents SAs and thus provides the IAV attachment factor for the interaction studies. Although “human” IAV strains, such as X31 (H3N2), are known to prefer α-2,6-linked over α-2,3-linked SAs,<sup>[37]</sup> it has been shown that the corresponding difference in binding affinity is only minor (with HA-SA dissociation constants of  $K_d \approx 2$  and 3 mM for α-2,6 and α-2,3 linkage, respectively).<sup>[38]</sup> Despite the fact that GD1a presents α-2,3-linked SAs, its use in IAV-SA interaction studies is therefore justified and is, for example, in line with the fact that HAI assays probing X31 binding inhibition have been done in the past with RBCs presenting any of the two linkages.<sup>[39,40]</sup>

In order to image the viruses, the envelope of the IAVs was labeled with the dye rhodamine octadecyl and TIRF microscopy was used to follow IAV attachment to/release from the SA-containing SLBs (Figure 2a). Single particle tracking (SPT) applied to the resulting TIRF microscopy videos allowed for tracking the motion of single viruses interacting with the SLB with high spatial accuracy (<15 nm) and subsequent application of the equilibrium fluctuation analysis (EFA)<sup>[41,42]</sup> yielded information on the rate of IAV attachment to the SLB, the IAV diffusion coefficient (which is a qualitative measure for the average

**Table 2.** Inhibitor performance in comparison of HAI and TIRF measurements.

	HAI $k_i$		TIRF IC <sub>50</sub>	
	[mol L <sup>-1</sup> ]	[μg mL <sup>-1</sup> ]	[mol L <sup>-1</sup> ]	[μg mL <sup>-1</sup> ]
hPG <sub>10</sub> -SA-SO <sub>4</sub>	82 × 10 <sup>-6</sup>	1214	2 × 10 <sup>-6</sup>	30
hPG <sub>100</sub> -SA-SO <sub>4</sub>	5 × 10 <sup>-6</sup>	685	0.6 × 10 <sup>-6</sup>	82
hPG <sub>500</sub> -SA-SO <sub>4</sub>	50 × 10 <sup>-9</sup>	35	0.4 × 10 <sup>-6</sup>	279
hPG <sub>2600</sub> -SA-SO <sub>4</sub>	31 × 10 <sup>-12</sup>	0.1	30 × 10 <sup>-12</sup>	0.1
hPG <sub>2600</sub> -SA	31 × 10 <sup>-12</sup>	0.1	3 × 10 <sup>-12</sup>	0.01
hPG <sub>2600</sub> -SO <sub>4</sub>	no inh.	no inh.	no inh.	no inh.

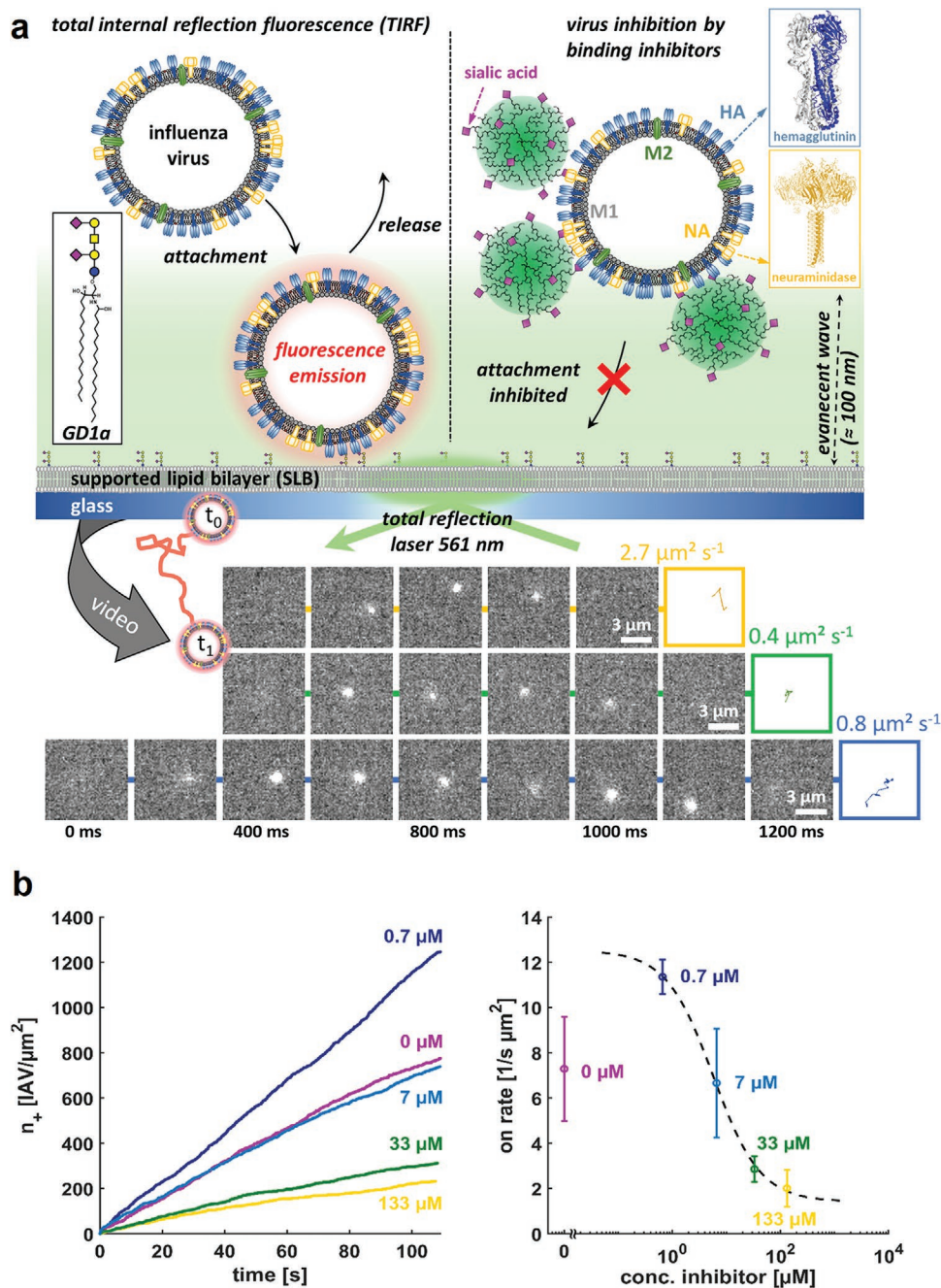


**Figure 2.** Experimental setup used to study IAV X31 binding to sialic acids (SAs) and the modification of this interaction upon addition of hPG inhibitors. a) Supported lipid bilayers (SLBs) containing the sialic acid-presenting ganglioside GD1a were used as artificial cell membranes. Fluorescently labeled IAVs (R18 dye incorporated in the virus envelope) bind to sialic acids exposed by the SLB, a process which is followed by TIRF imaging (always performed at room temperature; 20 °C). b) The cumulative number of newly arriving IAVs, as calculated using the EFA procedure, increases linearly with time. The slope of these traces is proportional to the rate of IAV attachment to the SA-containing SLB and allows for determining IAV binding inhibition upon addition of hPG inhibitors. The plot shows a representative example using the inhibitor hPG<sub>10</sub>-SA-SO<sub>4</sub>.

number of attachment factors bound by the tracked IAV), and the IAV residence time distribution as described previously.<sup>[35]</sup>

As the inhibitors were designed to prevent IAV binding to membranes, it is straightforward to assess their inhibition efficiency by quantifying the change of the rate of IAV attachment to the SA-presenting SLB as function of the inhibitor concentration (Figure 2b). According to the EFA procedure,<sup>[41,42]</sup> this rate

is extracted by calculating, for each recorded TIRF movie separately, the total number of IAVs that have been newly bound to the SLB since the beginning of the TIRF movie. Under equilibrium conditions (i.e., if SLB-bound and solution-dissolved viruses are in thermodynamic equilibrium) this number, the so-called cumulative number of newly arising viruses, increases linearly with measurement time, and the slope of this function

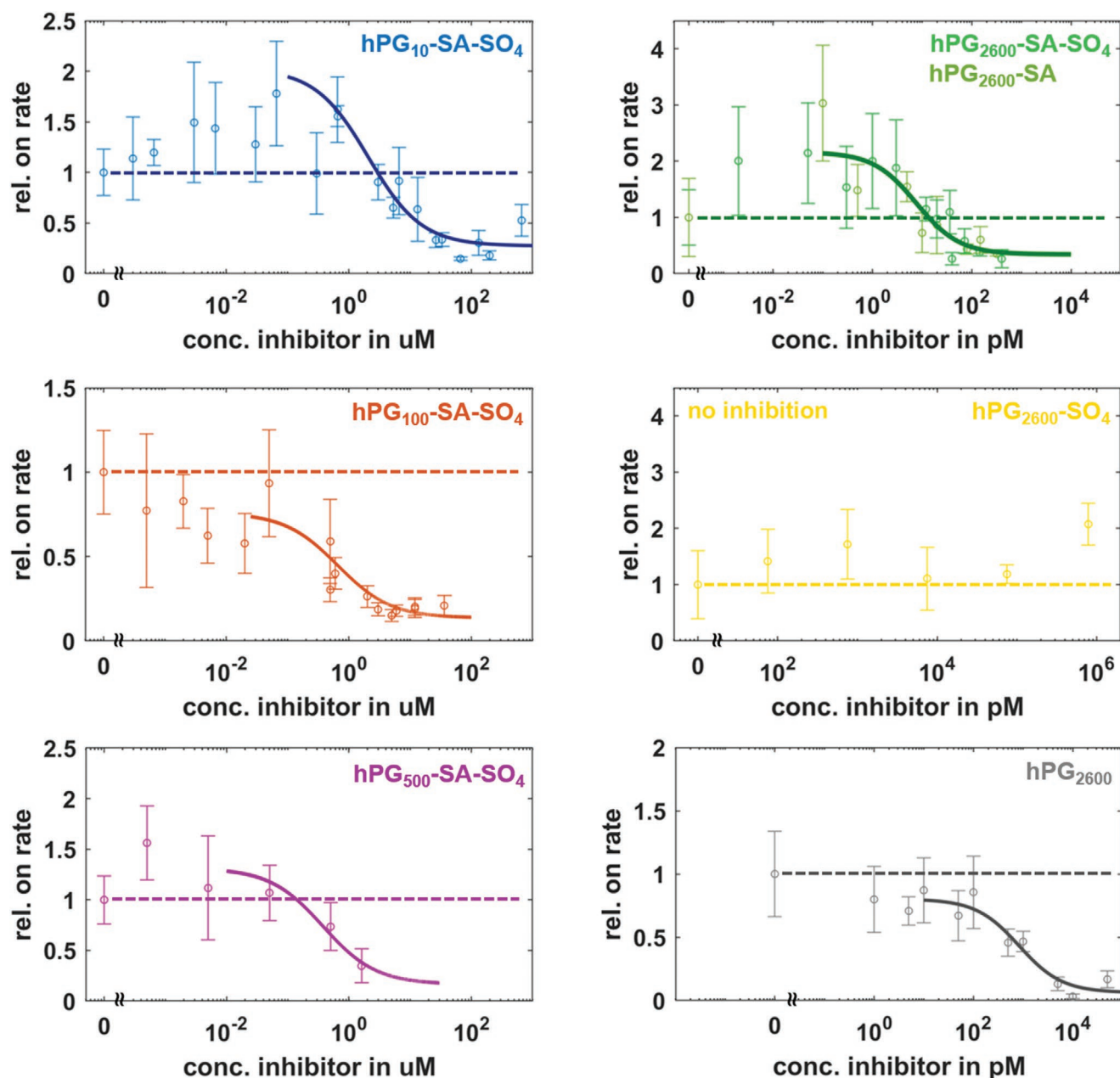


**Figure 3.** Change in IAV attachment rates upon hPG inhibitor (10, 100, 500, 2600 kDa) addition. Shown is the relative on-rate, which was calculated by normalizing the IAV attachment rate at a given hPG inhibitor concentration by the IAV attachment rate in absence of the inhibitor (i.e., at 0 m inhibitor concentration). Dashed lines are fixed to a relative on-rate value of one and thus show, if the rate of IAV attachment increases ( $>1$ ) or decreases ( $<1$ ) upon inhibitor addition. Surprisingly, both cases are observed for all SA-presenting inhibitors (except for the 100 kDa compound), generating a biphasic behavior in IAV binding inhibitor (see main text for details). Solid lines are fits of a Langmuir-type inhibition model to the data, allowing to determine the  $IC_{50}$  value of the inhibitors. Symbols indicate average values  $\pm$  standard deviation of at least five measurements.

corresponds to the IAV attachment rate for the area probed.<sup>[41,42]</sup> Addition of the inhibitors changed the slope of the cumulative number of newly arising IAVs, which indicates a change of the rate of IAV attachment to the SLB caused by the presence of the inhibitors (Figure 2b). Strong inhibition of IAV binding is reflected by a strong decrease in the IAV attachment rate, so that the change in the IAV attachment rate (with respect to its value in absence of any inhibitor) is indicative for the inhibition efficiency.<sup>[22]</sup> Hence, in the following all IAV attachment rates

will be normalized by the value in absence of any inhibitor, which is denoted as relative on-rate in this work.

As expected for binding inhibitors, all SA-presenting hPGs showed a decrease in the relative on-rate for a sufficiently large inhibitor concentration (Figure 3). Fitting a Langmuir-type inhibition curve to the relative on-rate in this concentration range allowed for determining the inhibitor concentration, at which the IAV binding rate to the SLB has been reduced by 50% (the so-called  $IC_{50}$  value; Table 2). While the 10 to 500 kDa

hPG inhibitors showed  $IC_{50}$  values in the  $\mu\text{M}$  molar range, the 2600 kDa hPG inhibitors reached  $\text{pM}$  values. This impressive value is not only due to the high molecular weight of these large inhibitors, but also by an improved inhibition potential as indicated when comparing the  $IC_{50}$  values expressed in mass concentrations (Table 2); compared to the smaller inhibitors, a virus inhibition is achieved for the 2600 kDa hPGs at a three order of magnitudes lower mass concentration, which is indicative for a multivalency-based enhancement of the inhibition. In addition, both SA-functionalized 2600 kDa hPGs showed comparable inhibition efficiency, that is, hPGs with SA and sulfate functionalization is not notably more effective than the inhibitor with just SA, while the one lacking SA but carrying sulfates did not show any IAV inhibition. Both observations are expected, as IAVs bind with much higher affinity to sialic acids than to sulfates, so that the interaction is dominated by sialic acids for the SA-containing inhibitors and negligible (for the inhibitor concentrations investigated) if only sulfates are present on the inhibitor.

As inhibition is only observed for inhibitors presenting SAs (which are known to be the IAV attachment factor) and as SA-presenting inhibitors (see Table 1) as well as SA-presenting bilayers are negatively charged,<sup>[43]</sup> IAV inhibition must be due to binding of the hPG-based inhibitors to the viruses. This conclusion is in line with the observations of related SA-presenting inhibitors and the measurement of size distributions of IAVs in presence and absence of the inhibitor (Figure S3, Supporting Information).<sup>[25]</sup>

In contrast, the non-functionalized MDa hPG also showed inhibition in the TIRF-based assay with an apparent  $IC_{50}$  value of  $\approx 1000 \text{ pM}$ , while no inhibition was observed in the HAI assay. We attribute this behavior to the slightly positive zeta potential (Table S1, Supporting Information) of this polymer, which promotes its binding to negatively charged sialic acid groups presented by the SLB and thus blocks the interaction between IAVs and the SLB by steric depletion of the attachment factors. This view is confirmed by the lack of any inhibition potential of  $\text{hPG}_{2600}\text{-SO}_4$ , which possesses, as all functionalized hPGs, a negative surface charge and is therefore not able to bind to the negatively charged SLB. A reason for its positive zeta potential of the non-functionalized MDa hPG could be the incorporation of salt ions although the polymer was excessively dialyzed against water. A treatment of the polymer solution with cation exchanger before the measurement of the zeta potential did not change the slightly positive zeta potential result. All functionalized hPGs showed the expected zeta potential, which verifies the measurement principle.

Nevertheless, for all SA-presenting inhibitors the results on IAV binding inhibition obtained using the HAI- or TIRF-based assays are qualitatively in good agreement (Table 2), although the TIRF-based assay reports in general slightly smaller  $IC_{50}$  values than the HAI-assay. Both assays show that the  $IC_{50}$  values generally decrease with increasing inhibitor size, that is, that the inhibitors become more potent for increasing size of its scaffold. This trend is in fact expected based on the theoretical considerations of Vonnemann et al.,<sup>[10]</sup> who show based on geometrical considerations that an optimal size for binding inhibitors exists. These considerations show that increasing the inhibitor size also increases the contact area between inhibitor

and virus and thus the virus-inhibitor interaction. Nevertheless, as the inhibitor mass also scales with the third power of the inhibitor size, this increase in inhibitor size also increases the applied mass concentration of the inhibitor, which partially cancels the enhancement caused by the increase in binding strength. Hence, there exists an optimum inhibitor size at which the lowest (total) mass of inhibitor is required for inhibition and which is, according to Vonnemann et al.<sup>[10]</sup> approximately one third of the size of the virus to be inhibited. As IAV X31 typically shows spatial extensions ranging between 80 and 120 nm, an optimum in binding inhibition is expected for inhibitor diameters on the order of 30 nm, which is realized by the MuVib inhibitor ( $\text{hPG}_{2600}\text{-SA-SO}_4$ , Table 1). In this context, the decrease of the  $IC_{50}$  value with increasing inhibitor size qualitatively matches to the predictions of Vonnemann et al.<sup>[10]</sup> A test, if the 2600 kDa MuVib inhibitor indeed achieves optimum inhibition efficiencies was, however, not possible, as this would have required to synthesize notably larger hPG scaffolds, which was not achievable in this study. A complementary approach to achieve related inhibitors with larger sizes is nanoprecipitation, in which smaller hPGs are crosslinked to form nanogels. For example, Bhatia et al. recently introduced hPG-based nanogel inhibitors with sizes of  $\approx 250 \text{ nm}$  and achieved  $IC_{50}$  values of about  $30 \mu\text{g mL}^{-1}$ .<sup>[25]</sup> This performance is two to three magnitudes lower than the one of the 2600 kDa MuVib inhibitor and indicates that the optimum inhibitor size for IAV binding inhibition is in between of 30 and 250 nm.

Nevertheless, while the HAI assay provides a rather binary readout (i.e., if the inhibitor concentration is sufficient to inhibit agglutination of red blood cells),<sup>[33]</sup> the changes in the IAV attachment rate measured by TIRF showed biphasic progression: Starting at small inhibitor concentrations ( $\ll IC_{50}$ ), the attachment rates first increased with increasing inhibitor concentration, followed by a saturation and a strong decrease at large inhibitor concentrations ( $\approx IC_{50}$ ). This surprising behavior indicated that the SA-functionalized hPG inhibitors promoted IAV attachment at relatively low inhibitor concentrations, while IAV binding inhibition was observed for sufficiently large inhibitor concentrations. The first phase (increase in IAV attachment rate) is not resolvable in the HAI-assay, as the IAV concentration is chosen such that IAV-induced agglutination is observed in absence of the inhibitor. This means that an increase in the IAV attachment rate to the cell membranes is not resolved by HAI, as in absence of inhibitors the IAV attachment rate is already sufficiently large to achieve agglutination.

This biphasic behavior, which was observed for all inhibitors except for  $\text{hPG}_{100}\text{-SA-SO}_4$  and which first increases the IAV binding rate to membranes at low inhibitor concentrations until a decrease is observed at large concentrations, was unexpected. Nevertheless, the observed increase in IAV attachment rate resembles changes to the IAV binding properties observed upon application of neuraminidase inhibitors.<sup>[35]</sup> Hence, the biphasic behavior suggests that at relatively low concentrations the inhibitors bind first to the NA and therefore act as NA inhibitors, while binding to HA and thus binding inhibition requires higher inhibitor concentrations. This interpretation is consistent with measurements on the affinity of the envelope proteins to sialosides,<sup>[44,45]</sup> showing that the dissociation constant  $K_d$  of the NA-SA interaction is 3 order of magnitude

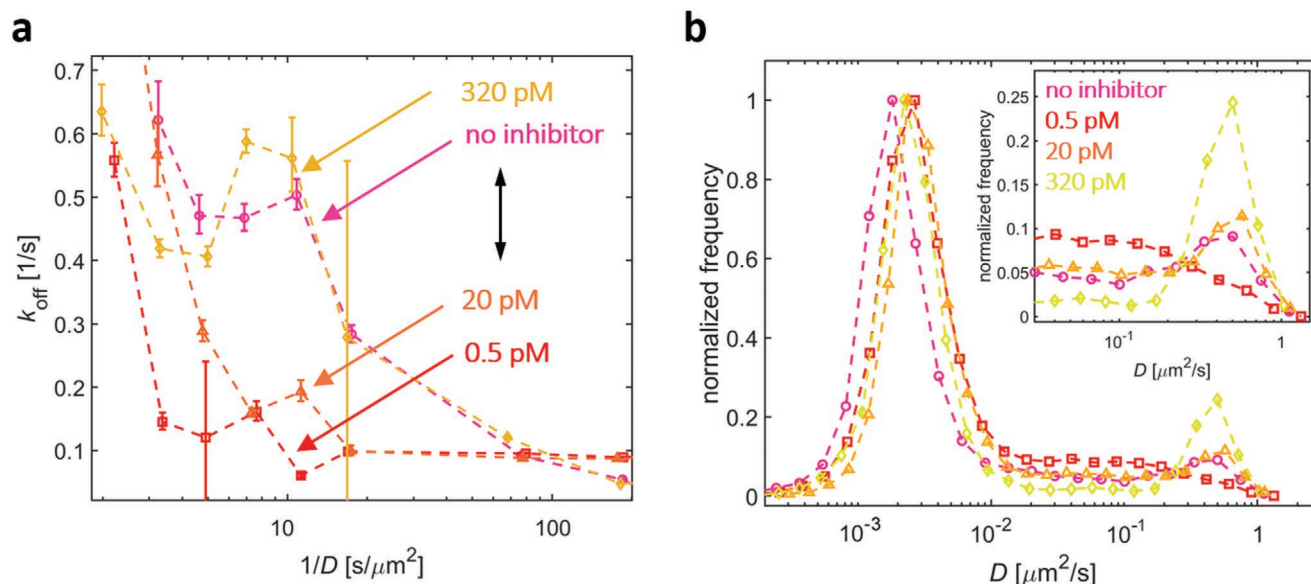


**Figure 4.** a) Changes of the IAV off-rate and b) diffusion coefficient distribution upon addition of the hPG<sub>2600</sub>-SA-SO<sub>4</sub> MuVib inhibitor. The biphasic binding behavior is also observed in these distribution, as addition of small amounts of the inhibitor ( $\leq 20$  pM) leads to a decrease in the off-rate distribution and a shift of the diffusion coefficient distribution from large to small values (indicating an increase in average binding valency), while addition of larger amounts of the inhibitor ( $>20$  pM) restores the off-rate distribution and shifts the diffusion coefficient distribution from small to large values (indicating an decrease in average binding valency).

smaller than the one of the HA-SA interaction ( $\approx \mu\text{M}$  vs.  $\approx \text{mM}$ , respectively) and supporting the hypothesis that also the inhibitors exhibit higher affinity (lower  $K_d$  value) towards NA than HA. Furthermore, evidence is accumulating that NA also contributes to the process of IAV binding to membranes.<sup>[33,46]</sup>

If the hypothesis is correct that the inhibitors bind preferentially to NA at relatively low inhibitor concentrations and to HA at sufficiently large ones, one would expect to see inhibitor concentration-dependent changes of the IAV off-rate and valency distribution, as both IAV binding properties strongly depend on the functional balance between HA and NA.<sup>[35]</sup> In order to test this hypothesis, we extracted IAV off-rate and valency distributions from the TIRF measurements as recently described.<sup>[35]</sup> In brief, here we make use of the fact that the diffusion coefficient of SLB-bound IAVs,  $D$ , decreases with increasing valency (=number of bound GD1a gangliosides), so that the changes to the IAV valency distribution also induce changes to the distribution of IAV diffusion coefficients. Although the exact relationship connecting IAV valency and diffusion coefficient has not yet been resolved, all theoretical models indicate that both properties are connected by a monotonously decreasing function, that is, large values of the diffusion coefficient correspond to a small value of the average valency and vice versa.<sup>[47]</sup> Furthermore, the measurement of the IAV diffusion coefficient also allows to deconvolute the IAV residence time distribution from valency effects, yielding valency-resolved off-rate distributions.<sup>[35]</sup>

In absence of any inhibitor (open circles, **Figure 4a**), the observed off-rate distribution is dominated by a decrease for increasing apparent average valency  $D^{-1}$ , but also shows a peak structure, leading to elevated off-rates at intermediate average valencies ( $D^{-1} \approx 8 \text{ s } \mu\text{m}^{-2}$ ). The presence of a peak structure matches to previous observations,<sup>[35]</sup> in which it is shown that

this structure is caused by the opposing functionalities of HA and NA and vanishes upon application of NA inhibitors such as zanamivir. Furthermore, the addition of zanamivir also increased the rate of IAV attachment and both effects together yielded a strong increase in the number of bound IAVs. Interestingly, exactly the same behavior is observed here at relatively low inhibitor concentrations, at which the relative IAV on-rate increases (Figure 3) and the IAV off-rate decreases with increasing inhibitor concentration (open triangles and squares, Figure 4a). Hence, at relatively low concentrations, the inhibitors behave like a NA inhibitor with respect to the induced changes in IAV attachment and off-rate distribution.

Additional evidence is provided by the diffusion coefficient distributions (Figure 4b), which showed a shift from large to small values upon addition of small amounts of the inhibitor ( $\ll \text{IC}_{50}$ ) and a shift from small to large diffusion coefficient values upon addition of large amounts of the inhibitor ( $\gg \text{IC}_{50}$ ). As the diffusion coefficient  $D$  is indicative for the average valency of the IAV-SA interaction, these changes indicate that the addition of inhibitors modifies the IAV valency distribution. In particular, the shift from large to small  $D$ -values observed for inhibitor concentrations below  $\text{IC}_{50}$  indicates an increase of the average binding valency ("NA-like inhibition"), while the opposite behavior is observed above  $\text{IC}_{50}$  and thus indicates a decrease in average binding valency ("HA inhibition"). There is, however, a lower limit for the valency, below which the interaction of the IAV to the membrane becomes too small to maintain IAV binding to the membrane. This limit is reached for  $D$ -values exceeding  $\approx 1 \mu\text{m}^2 \text{ s}^{-1}$ , so that the  $D$ -distributions exhibit an edge at  $\approx 1 \mu\text{m}^2 \text{ s}^{-1}$  and, in connection with the transfer of events from small to large  $D$ -values, a peak-like structure, which raises with increasing inhibitor concentration added.



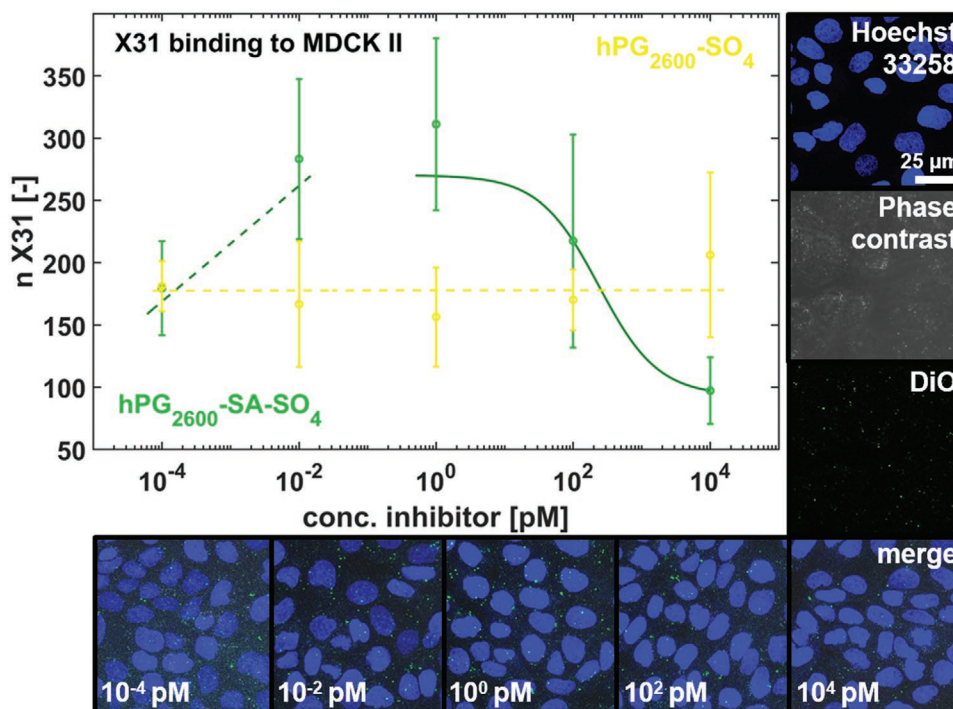


**Figure 5.** Inhibition of IAV X31 binding to MDCK II cells upon addition of the hPG<sub>2600</sub>-SA-SO<sub>4</sub> MuVib inhibitor (green symbols) and of the negative control hPG<sub>2600</sub>-SO<sub>4</sub> (yellow symbol). The cell-based assay also shows a biphasic change of IAV binding inhibition as observed in the TIRF-based binding assay. IAVs were labeled with DiO (green structures in the cell images), while the MDCK II cells were labeled using Hoechst 33258 (blue structures). Symbols indicate average values  $\pm$  standard deviation of four measurements. Dashed lines are to guide the eye.

Nevertheless, in order to probe, if the phenomenon of increased IAV attachment rates at small inhibitor concentrations ( $\ll$ IC<sub>50</sub>) can also be observed for native cell plasma membranes, we further investigated the IAV binding to MDCK-II cells, which are known to expose  $\alpha$ -2,6-linked and  $\alpha$ -2,3-linked SAs and are an established cell line for investigating IAV binding to and infection of cells.<sup>[48]</sup> Here, labelled IAVs were mixed with different concentration of the inhibitor hPG<sub>2600</sub>-SA-SO<sub>4</sub> at room temperature for 45 min. Afterwards, the virus-inhibitor mixture was incubated with MDCK-II cells for 2 h on ice. Non-bound IAVs were removed by washing twice with PBS buffer, while bound IAVs remained at the cell surface. Using confocal laser scanning microscopy Z-wide images of the cell layer were taken and stacked to visualize all viruses at the cell surface, followed by quantifying the number of bound viruses using ImageJ.<sup>[49]</sup> The number of MDCK-II cell-bound IAVs (**Figure 5**) showed the same dependence of the inhibitor concentration as the relative on-rate determined using TIRF microscopy (Figure 3), verifying an increased IAV attachment at low concentrations and a decrease in IAV attachment at higher concentrations. The sulfated derivative (hPG<sub>2600</sub>-SO<sub>4</sub>) was used as negative control and showed no impact on the IAV binding. Hence, the biphasic change in the IAV binding behavior upon inhibitor addition is observed for IAVs interacting with attachment factor-equipped SLBs as well as with cell membranes, which further supports our view that these inhibitors behave as NA-like inhibitors at low inhibitor concentrations and as HA inhibitors at high concentrations. Furthermore, as MDCK-II cells present  $\alpha$ -2,6-linked as well as  $\alpha$ -2,3-linked SAs, obtaining

the same inhibition curve as in the TIRF assay post-validates that GD1a is a suitable attachment factor for probing the interactions between IAV X31 and GD1a.

### 3. Conclusions

In this study, hyperbranched polyglycerol (hPG)-based virus binding inhibitors have been synthesized, the size and functionalization of which have been inspired from mucins. The resulting mucin-inspired virus binding (MuVib) inhibitor was based on a 2.6 MDa hPG core that was functionalized with sialic acids and sulfate groups (5 mol% of the hPGs OH groups, respectively). In addition, hPG-based inhibitors having the same functionalization but lower molecular weights (ranging between 10 and 2600 kDa) were synthesized as well, which allowed to probe the impact of the inhibitor size on its inhibition efficiency. This efficiency of the synthesized compounds in inhibiting the binding of a common respiratory virus, a H3N2 influenza A virus (IAV), was assessed using a cell binding and the hemagglutination inhibition assay, both of which provide information about the minimum inhibitor concentration that needed to inhibit IAV binding to membranes. Furthermore, a recently developed TIRF-based assay was employed to quantify, how inhibitor addition modified the multivalent interaction arising between IAVs and their native attachment factor, sialic acids.

Surprisingly, the inhibition of IAV binding to membranes showed a biphasic behavior for increasing inhibitor concentrations: At relatively low inhibitor concentrations, the IAV binding

first increased with increasing inhibitor concentrations, followed by a second regime at higher inhibitor concentrations, at which the expected decrease in IAV binding was observed for increasing inhibitor concentrations. The results of the TIRF-based assay and the cell binding assay indicate that the inhibitors bind at low inhibitor concentrations preferentially to the IAV envelope protein neuraminidase (NA), leading to an enhancement of the IAV binding to lipid membranes, while at larger inhibitor concentrations, it binds additionally to another IAV envelope protein, hemagglutinin (HA), causing IAV binding inhibition. Potent inhibition of IAV binding (HA inhibition) by the 2600 kDa MuVib inhibitor is observed in all these assays already at  $\mu\text{M}$  concentrations, while decreasing the molecular weight of the inhibitors decreased their inhibition efficiency (increase in their  $\text{IC}_{50}$  value), which is in qualitative agreement with the prediction by a recent study of Vonnemann et al.<sup>[10]</sup>

#### 4. Experimental Section

**Synthesis of High-Molecular Weight hPG:** The synthesis of the MDa hPG was performed in two steps,<sup>[16]</sup> as previous investigations showed that using one step approaches the molecular weight of hPGs can be increased to only 800–900 kDa.<sup>[17,50]</sup> This limitation has been attributed in the past to the decrease in the concentration of active alkoxide units on polyglycerol, which are key elements to chain/branching and propagation of the hPG systems.<sup>[51]</sup>

First, a macroinitiator was synthesized in a heterogenous reaction mixture in dioxane. Dry trimethylolpropane (120 mg, 0.89 mmol, 1.0 eq.) was partially deprotonated (30% OH) with potassium methoxide (67  $\mu\text{L}$ , 0.27 mmol, 0.3 equiv., 25% in methanol) in argon atmosphere at 60 °C for 30 min. After the addition of 24 mL dioxane (dry) the turbid mixture was heated to 100 °C. Glycidol (12 mL, 0.18 mol, 201 equiv.) was slowly added (0.5 mL  $\text{h}^{-1}$ ) via syringe pump into the reaction mixture. The polymer was purified by removing the dioxane, precipitation as methanolic solution in acetone and dialysis against water in regenerated cellulose membrane (10 kDa MWCO). The resulted hPG (Mn: 600 kDa,  $\bar{D}$  1.1) was obtained with a yield of 93.6 %.

In the second step, this hPG was used as macroinitiator to grow the polymer further. 2.5 g (0.034 mol, total OH groups) of the lyophilized polymer was dissolved in dry DMF (35 mL). The polymer was partially deprotonated with the addition of potassium hydride in oil (30 wt%) (80  $\mu\text{g}$ , 272  $\mu\text{L}$ , 2.0  $\mu\text{mol}$ ). The temperature was increased to 100 °C and glycidol (25 mL, 0.37 mol) were added with a rate of 0.9 mL  $\text{h}^{-1}$ . After precipitation in acetone and dialysis against water in regenerated cellulose membrane (50 kDa MWCO) the resulted molecular weight was 2.6 MDa with a  $\bar{D}$  of 1.4.

**Mesylation and Azidation:** Both reactions were performed sequentially in one pot. 1300 mg hPG (2.6 MDa) (0.88 mol OH to be functionalized) was dissolved in dry DMF (18 mL). The mesylation was done with methanesulfonyl chloride (201 mg, 1.8 mmol, 2.0 eq.) in the presence of triethyl amine (306  $\mu\text{L}$ , 2.2 mmol, 2.5 mol eq.) at room temperature for 16 h. Afterwards the azidation was directly performed by the addition of sodium azide (456 mg, 7.0 mmol, 8 equiv.) at 80 °C for 20 h under argon atmosphere. Purification was done by dialysis against water (2 kDa MWCO, benzoylated). The product was analyzed by  $^1\text{H}$  NMR and elemental analysis to determine the amount of introduced azide groups (see Figure S5, Supporting Information).

**Sulfation:** The azidated hPG (400 mg, 0.27 mmol OH to be functionalized, 1.0 equiv.) was sulfated using sulfur trioxide pyridine complex (55.9 mg, 0.4 mmol, 1.3 equiv.) in dry DMF (12 mL) at 60 °C for 20 h under argon atmosphere. After the reaction time was over the pH value was increased to pH 10 by the addition of sodium hydroxide solution (0.3 mol  $\text{L}^{-1}$ ). The product was dialyzed against sodium hydroxide solution (0.3 mol  $\text{L}^{-1}$ ), 10 wt% NaCl and water. The yield of the

sulfation was analyzed by elemental analysis. Further, a  $^1\text{H}$  NMR of the product was performed (see Figure S6, Supporting Information).

**Click Protected Propagated Sialic Acid by CuAAC:** The sulfated polymer hPG<sub>2600</sub>-N<sub>3</sub>-SO<sub>4</sub> (150 mg, 0.11 mmol OH to be functionalized, 1.0 equiv.) was mixed with acetyl protected propagated sialic acid (72.9 mg, 1.3 mmol, 1.2 equiv.) in DMF. Copper sulfate pentahydrate (11.1 mg, 0.04 mmol, 0.4 equiv.) and sodium-L-ascorbate (88.3 mg, 0.4 mmol, 4 equiv.) were dissolved separately in a small amount of water and combined afterwards. The solution was transferred to the polymer solution. The reaction was performed at 50 °C for 20 under argon atmosphere. Infrared spectroscopy indicated complete conversion by the disappearance of the azide band (2100  $\text{cm}^{-1}$ ; see Figure S7, Supporting Information) within the resolution limit of the instrument (determined by multiple repetitions of the measurement and calculation of the standard error). Hence, it is reasonable to assume that the functional degree of conjugated sialic acid is almost the same as the initial degree of azidation ( $\approx 5\text{--}7\%$ ). The pH value was increased to pH 10 with sodium hydroxide solution (2 mol  $\text{L}^{-1}$ ) to cleave the acetyl protection of the sialic acid within 2 h. EDTA disodium salt (14.0 mg, 0.04 mmol, 0.4 equiv.) was added to improve the removal of copper ions during dialysis against water. The purified polymer was analyzed by  $^1\text{H}$  NMR (see Figure S9, Supporting Information) and elemental analysis.

The synthesized virus binding inhibitors were characterized in regard to size with dynamic light scattering (DLS) and in respect of surface charge by zeta potential measurements.

**Dynamic Light Scattering:** The hydrodynamic diameter was measured by dynamic light scattering at a concentration of 1 mg  $\text{mL}^{-1}$  in PBS buffer using Zetasizer Nano series ( $\lambda = 532\text{ nm}$ ) from Malvern Panalytical (Kassel, Germany). Disposable cuvettes (ZEN0040) from Brand (Wertheim, Germany) out of polystyrene were used. Before the measurement all samples were filtered through a 0.2  $\mu\text{m}$  Minisart RC 15 syringe filter from Satorius (Göttingen, Germany). Temperature equilibration was done for 1 min at 25 °C. The measurements were performed for ten scans each 15 s in back scattering mode (173°). The stated values result from at least three measurements.

**Zeta-Potential:** The surface charge was investigated by zeta-potential measurement with Zetasizer Nano series ( $\lambda = 532\text{ nm}$ ) using folded capillary zeta cells (DTS 1070) from Malvern Panalytical (Kassel, Germany). The sample concentration was 1 mg  $\text{mL}^{-1}$  in 10 mm phosphate buffer solution (0.411 g  $\text{L}^{-1}$   $\text{Na}_2\text{HPO}_4$ , 0.178 g  $\text{L}^{-1}$   $\text{KH}_2\text{PO}_4$ , pH 7.4). All samples were filtered through a 0.2  $\mu\text{m}$  Minisart RC 15 syringe filter from Satorius (Göttingen, Germany). Five measurements with ten scans (each 15 s) were done to obtain the zeta potential based on the Smoluchowski model.

The virus binding performance was investigated by two independent methods: hemagglutination inhibition (HAI) assay and total internal reflection fluorescence (TIRF) microscopy.

**Hemagglutination Inhibition Assay:** The inhibitors were two-fold diluted with PBS in a v-shaped microtiter plate. Afterwards, 2 HA X31 virus were transferred to each inhibitor dilution. After 30 min incubation time at room temperature 50  $\mu\text{L}$  of 1% chicken RBC solution (Robert Koch-Institute, Berlin) was added to each well. Then, it was incubated for 60 min at room temperature before the read out was done. The lowest concentration where the sedimentation of red blood cells was still inhibited by hemagglutination represents the inhibitor constant  $k_i$  (see Figure S2, Supporting Information).

**Total Internal Reflection Fluorescent Microscopy:** Single virus tracking was done on a supported lipid bilayer (SLB), which represents the cell surface. IAV bind in a multivalent fashion to incorporated GD1a gangliosides (1 mol%). Extruded vesicles out of POPC and 1 mol% GD1a were exposed in an aqueous solution (0.33 mg  $\text{mL}^{-1}$ ) on a cleaned glass, absorb, deform, and form a cohesive supported lipid bilayer by rupturing on the glass surface. Sialic acids on the GD1a are the natural target of IAVs. After 10 min excess vesicles were removed by washing with PBS buffer. Then, IAV solution with or without containing binding inhibitor was injected. Through excitation in TIRF mode, an evanescent light beam (white light + m-cherry filter) penetrates approximately 100 nm in the solution and reaches therefore just bound viruses ( $\approx 100\text{ nm}$ ) on

the membrane. This ensures that rhodamine (R18) labeled viruses in the evanescent region get excited and emit light, non-bound labeled virus in the solution are not visible. Videos with 0.11 fps were taken to visualize the virus attachment, diffusion and detachment on the GD1a receptor containing SLB. The videos were analyzed by homemade MATLAB scripts using equilibrium fluctuation analysis (EFA).

**IAV Binding to MDCK-II Cells:** The cultured MDCK II cells were seeded in 8-well confocal slides and cultured for 1–2 days till confluency. 100  $\mu$ L X31 solution (protein content: 0.36mg mL<sup>-1</sup>, 1.1  $\times$  10<sup>11</sup> particles mL<sup>-1</sup>) was incubated with 2  $\mu$ L of 20  $\mu$ M DiO (in ethanol, D4929 in Merck, Darmstadt, Germany) for 30 min in dark. The free dyes were removed by spin column then. A mixture of 90  $\mu$ L inhibitor (in PBS) and 10  $\mu$ L labelled virus was added after 45 min at room temperature on the cell layer (culture medium was removed before by washing with PBS twice). After an incubation for 2 h on ice, non-binding viruses were removed by washing twice with PBS. The cell nucleus was labelled with Hoechst 33258 and the cells fixed with 4% paraformaldehyde. Finally, Z-wide images were taken with confocal laser scanning microscopy from the whole cell layer (30 images, step size 0.4  $\mu$ m). The number of binding viruses was determined from the stacked images using ImageJ.

## Supporting Information

Supporting Information is available from the Wiley Online Library or from the author.

## Acknowledgements

This work was supported by the German Research Foundation (BL1514/1-1 and project A6 within the CRC 765) and by the Focus Area NanoScale (Freie Universität Berlin). The authors thank the core facility BioSupraMol and the Macromolecular Hub (CBR) for the use of their research facilities. J.N.K. acknowledges the funding by Canadian Institutes of Health Research (CIHR), Natural Sciences and Engineering Council of Canada (NSERC) and Canada Foundation for Innovation (CFI). J.N.K. holds a Career Investigator Scholar award from the Michael Smith Foundation for Health Research (MSFHR). S.A. acknowledges a MSFHR postdoctoral fellowship.

Open access funding enabled and organized by Projekt DEAL.

## Conflict of Interest

The authors declare no conflict of interest.

## Keywords

hyperbranched polyglycerol, influenza A viruses, single particle tracking, TIRF microscopy, virus binding inhibition

Received: July 30, 2020

Revised: September 28, 2020

Published online: November 1, 2020

- [1] M. Hoffmann, H. Kleine-Weber, S. Schroeder, N. Kruger, T. Herrler, S. Erichsen, T. S. Schiergens, G. Herrler, N. H. Wu, A. Nitsche, M. A. Muller, C. Drosten, S. Pohlmann, *Cell* **2020**, 181, 271.  
 [2] C. V. Ventura, M. Maia, V. Bravo-Filho, A. L. Góis, R. Belfort, *Lancet* **2016**, 387, 228.  
 [3] G. Neumann, T. Noda, Y. Kawaoka, *Nature* **2009**, 459, 931.  
 [4] E. De Clercq, G. Li, *Clin. Microbiol. Rev.* **2016**, 29, 695.

- [5] C. Fasting, C. A. Schalley, M. Weber, O. Seitz, S. Hecht, B. Kokschi, J. Dornedde, C. Graf, E. W. Knapp, R. Haag, *Angew. Chem. Int. Ed. Engl.* **2012**, 51, 10472.  
 [6] L. L. Kiessling, J. E. Gestwicki, L. E. Strong, *Curr. Opin. Chem. Biol.* **2000**, 4, 696.  
 [7] M. Mammen, S. K. Choi, G. M. Whitesides, *Angew. Chem. Int. Ed. Engl.* **1998**, 37, 2754.  
 [8] A. Mulder, J. Huskens, D. N. Reinhoudt, *Org. Biomol. Chem.* **2004**, 2, 3409.  
 [9] M. Marsh, A. Helenius, *Cell* **2006**, 124, 729.  
 [10] J. Vonnemann, S. Liese, C. Kuehne, K. Ludwig, J. Dornedde, C. Bottcher, R. R. Netz, R. Haag, *J. Am. Chem. Soc.* **2015**, 137, 2572.  
 [11] J. Witten, T. Samad, K. Ribbeck, *Curr. Opin. Biotechnol.* **2018**, 52, 124.  
 [12] J. V. Fahy, B. F. Dickey, *N. Engl. J. Med.* **2010**, 363, 2233.  
 [13] R. Bansil, B. S. Turner, *Curr. Opin. Colloid Interface Sci.* **2006**, 11, 164.  
 [14] J. D. Reuter, A. Myc, M. M. Hayes, Z. Gan, R. Roy, D. Qin, R. Yin, L. T. Piehler, R. Esfand, D. A. Tomalia, *Bioconjugate Chem.* **1999**, 10, 271.  
 [15] M. Calderón, M. A. Quadir, S. K. Sharma, R. Haag, *Adv. Mater.* **2010**, 22, 190.  
 [16] P. Anilkumar, T. B. Lawson, S. Abbina, J. T. Mäkelä, R. C. Sabatelle, L. E. Takeuchi, B. D. Snyder, M. W. Grinstaff, J. N. Kizhakkedathu, *Nat. Commun.* **2020**, 11, 2139.  
 [17] M. I. ul-Hag, R. A. Sheno, D. E. Brooks, J. N. Kizhakkedathu, *J. Polym. Sci., Part A: Polym. Chem.* **2013**, 51, 2614.  
 [18] R. A. Cone, *Adv. Drug Deliv. Rev.* **2009**, 61, 75.  
 [19] N. K. Sauter, J. E. Hanson, G. D. Glick, J. H. Brown, R. L. Crowther, S. J. Park, J. J. Skehel, D. C. Wiley, *Biochemistry* **1992**, 31, 9609.  
 [20] M. A. Tortorici, A. C. Walls, Y. Lang, C. Wang, Z. Li, D. Koerhuis, G. J. Boons, B. J. Bosch, F. A. Rey, R. J. de Groot, D. Velesler, *Nat. Struct. Mol. Biol.* **2019**, 26, 481.  
 [21] G. H. Guibinga, A. Miyano, J. D. Esko, T. Friedmann, *Mol. Ther.* **2002**, 5, 538.  
 [22] N. Peerboom, E. Schmidt, E. Trybala, S. Block, T. Bergstrom, H. P. Pace, M. Bally, *ACS Infect. Dis.* **2018**, 4, 944.  
 [23] R. E. Loomis, A. Prakobphol, M. J. Levine, M. S. Reddy, P. C. Jones, *Arch. Biochem. Biophys.* **1987**, 258, 452.  
 [24] J. Bolscher, E. Veerman, A. Van Nieuw Amerongen, A. Tulp, D. Verwoerd, *Biochem. J.* **1995**, 309, 801.  
 [25] S. Bhatia, M. Hilsch, J. L. Cuellar Camacho, K. Ludwig, C. Nie, B. Parshad, M. Wallert, S. Block, D. Lauster, C. Böttcher, *Angew. Chem., Int. Ed.* **2020**, 59, 12417.  
 [26] S. Bhatia, D. Lauster, M. Bardua, K. Ludwig, S. Angioletti-Uberti, N. Popp, U. Hoffmann, F. Paulus, M. Budt, M. Stadtmüller, *Biomaterials* **2017**, 138, 22.  
 [27] D. Lauster, S. Klenk, K. Ludwig, S. Nojumi, S. Behren, L. Adam, M. Stadtmüller, S. Saenger, S. Zimmmer, K. Hönzke, L. Yao, U. Hoffmann, M. Bardua, A. Hamann, M. Witzernath, L. E. Sander, T. Wolff, A. C. Hocke, S. Hippenstiel, S. De Carlo, J. Neudecker, K. Osterrieder, N. Budisa, R. R. Netz, C. Böttcher, S. Liese, A. Herrmann, C. P. R. Hackenberger, *Nat. Nanotechnol.* **2020**, 15, 373.  
 [28] E. de Vries, W. Du, H. Guo, C. A. M. de Haan, *Trends Microbiol.* **2020**, 28, 57.  
 [29] P. E. Hamming, N. J. Overeem, J. Huskens, *Chem. Sci.* **2019**, 11, 27.  
 [30] R. Wagner, M. Matrosovich, H. D. Klenk, *Rev. Med. Virol.* **2002**, 12, 159.  
 [31] H. Guo, H. Rabouw, A. Slomp, M. Dai, F. van der Vegt, J. W. M. van Lent, R. McBride, J. C. Paulson, R. J. de Groot, F. J. M. van Kuppeveld, E. de Vries, C. A. M. de Haan, *PLoS Pathog.* **2018**, 14, e1007233.  
 [32] A. Harris, G. Cardone, D. C. Winkler, J. B. Heymann, M. Brecher, J. M. White, A. C. Steven, *Proc. Natl. Acad. Sci. U. S. A.* **2006**, 103, 19123.  
 [33] J. L. McAuley, B. P. Gilbertson, S. Trifkovic, L. E. Brown, J. L. McKimm-Breschkin, *Front. Microbiol.* **2019**, 10, 39.  
 [34] J. C. Pedersen, *Avian Influenza Virus*, Springer, Berlin, **2008**, pp. 53–66.

- [35] M. Müller, D. Lauster, H. H. K. Wildenauer, A. Herrmann, S. Block, *Nano Lett.* **2019**, *19*, 1875.
- [36] D. Axelrod, *Methods Cell Biol.* **1989**, *30*, 245.
- [37] T. Ito, Y. Kawaoka, *Vet. Microbiol.* **2000**, *74*, 71.
- [38] N. K. Sauter, M. D. Bednarski, B. A. Wurzburg, J. E. Hanson, G. M. Whitesides, J. J. Skehel, D. C. Wiley, *Biochemistry* **1989**, *28*, 8388.
- [39] M. Mammen, G. Dahmann, G. M. Whitesides, *J. Med. Chem.* **1995**, *38*, 4179.
- [40] J. Martín, S. A. Wharton, Y. P. Lin, D. K. Takemoto, J. J. Skehel, D. C. Wiley, D. A. Steinhauer, *Virology* **1998**, *241*, 101.
- [41] D. W. Lee, H. L. Hsu, K. B. Bacon, S. Daniel, *PLoS One* **2016**, *11*, e0163437.
- [42] M. Bally, A. Gunnarsson, L. Svensson, G. Larson, V. P. Zhdanov, F. Hook, *Phys. Rev. Lett.* **2011**, *107*, 188103.
- [43] R. McDaniel, K. Sharp, D. Brooks, A. McLaughlin, A. Winiski, D. Cafiso, S. McLaughlin, *Biophys. J.* **1986**, *49*, 741.
- [44] X. Zhu, R. McBride, C. M. Nycholat, W. Yu, J. C. Paulson, I. A. Wilson, *J. Virol.* **2012**, *86*, 13371.
- [45] R. E. Amaro, P. U. Ieong, G. Huber, A. Dommer, A. C. Steven, R. M. Bush, J. D. Durrant, L. W. Votapka, *ACS Cent. Sci.* **2018**, *4*, 1570.
- [46] J. Yang, S. Liu, L. Du, S. Jiang, *Rev. Med. Virol.* **2016**, *26*, 242.
- [47] S. Block, *Biomolecules* **2018**, *8*, 30.
- [48] S. Hatakeyama, Y. Sakai-Tagawa, M. Kiso, H. Goto, C. Kawakami, K. Mitamura, N. Sugaya, Y. Suzuki, Y. Kawaoka, *J. Clin. Microbiol.* **2005**, *43*, 4139.
- [49] C. Nie, B. Parshad, S. Bhatia, C. Cheng, M. Stadtmüller, A. Oehrl, Y. Kerkhoff, T. Wolff, R. Haag, *Angew. Chem. Int. Ed.* **2020**, *59*, 15532.
- [50] R. K. Kainthan, E. B. Muliawan, S. G. Hatzikiriakos, D. E. Brooks, *Macromolecules* **2006**, *39*, 7708.
- [51] D. Wilms, F. Wurm, J. Nieberle, P. Bohm, U. Kemmer-Jonas, H. Frey, *Macromolecules* **2009**, *42*, 3230.